Supplementary Materials for:

Structures of complete HIV-1 TAR RNA portray a dynamic platform poised for protein binding and structural remodeling

Charles Bou-Nader, Katie A. Link, Krishna C. Suddala, Jay R. Knutson, and Jinwei Zhang.

Supplementary Tables 1-5

Supplementary Figures 1-10

RNA	IC_{50} (nM)
VA-I	11 ± 3
TAR^{2GC} (WT)	77 ± 10
$TAR^{\Delta 4bp}$	N.D.
$TAR^{\Delta 9bp}$	N.D.
$TAR^{\Delta 14bp}$	N.D.
$TAR^{\Delta 23\text{-}39}$	387 ± 11
$TAR^{\Delta C5/\Delta A17}$	90 ± 9
$TAR^{\Delta 23UCU25}$	417 ± 30
$TAR^{\Delta C5/\Delta A17/\Delta 23UCU25}$	16 ± 6
$TAR^{A48U/C49G/U50A}$	1683 ± 76

Supplementary Table 1. Summary of IC_{50} measurements in PKR inhibition assays.
Values are mean ± s.d. of n= 3 biologically independent replicates. N.D.: not determined due to weak inhibition.

Method	Sample in Cell	Titrant	K_d (μM)	Log (K_a)	ΔH (kcal.mol^{-1})
FP	VA-I	PKR	0.04 ± 0.002	7.4 ± 0.02	-
	TAR^{2GC} (WT)		0.035 ± 0.005	7.46 ± 0.06	
	TAR$^{\Delta 4bp}$		0.05 ± 0.003	7.34 ± 0.03	
	TAR$^{\Delta 9bp}$		0.13 ± 0.04	6.85 ± 0.11	
	TAR$^{\Delta 14bp}$		1.23 ± 1	6.03 ± 0.4	
	TAR$^{\Delta 23\text{-}39}$		0.054 ± 0.01	7.26 ± 0.01	
	TAR$^{\Delta C5/\Delta A17}$		0.06 ± 0.003	7.22 ± 0.02	
	TAR$^{\Delta 23UCU25}$		0.05 ± 0.007	7.34 ± 0.06	
	TAR $^{\Delta C5/\Delta A17/\Delta 23UCU25}$		0.02 ± 0.03	7.65 ± 0.01	
	TAR$^{A48U/C49G/U50A}$		0.02 ± 0.03	7.02 ± 0.11	
	VA-I	dsRBMs	0.22 ± 0.08	6.69 ± 0.18	
	TAR^{2GC} (WT)		0.12 ± 0.01	6.91 ± 0.04	
	TAR$^{\Delta 4bp}$		0.29 ± 0.02	6.54 ± 0.03	
	TAR$^{\Delta 9bp}$		1.9 ± 0.7	5.74 ± 0.17	
	TAR$^{\Delta 14bp}$		2.28 ± 0.7	5.65 ± 0.13	
	TAR$^{\Delta 23\text{-}39}$		0.19 ± 0.03	6.73 ± 0.06	
	TAR$^{\Delta C5/\Delta A17}$		0.12 ± 0.01	6.91 ± 0.04	
	TAR$^{\Delta 23UCU25}$		0.14 ± 0.01	6.86 ± 0.03	
	TAR $^{\Delta C5/\Delta A17/\Delta 23UCU25}$		0.07 ± 0.02	7.17 ± 0.13	
	TAR$^{A48U/C49G/U50A}$		0.36 ± 0.12	6.46 ± 0.17	
ITC	TAR^{2GC} (WT)	HIV-1 Tat$^{44\text{-}60}$ WT	0.16 ± 0.1	6.82 ± 0.2	-11.5 ± 1.7
	TAR^{GAAA}		0.6 ± 0.18	6.29 ± 0.14	-6.8 ± 0.7
	TAR$^{G21C/C41G}$		0.65 ± 0.2	6.21 ± 0.16	-9.6 ± 1
	TAR$^{A22U/U40A}$		0.67 ± 0.11	6.18 ± 0.08	-10.8 ± 0.6
	TAR^{U23C}		N.D.		
	TAR^{U23A}		N.D.		
	TAR^{C24U}		0.07 ± 0.07	7.3 ± 0.4	-11.4 ± 0.4
	TAR^{C24G}		0.1 ± 0.04	7.0 ± 0.16	-12.5 ± 0.6
	TAR^{C24A}		0.3 ± 0.1	6.5 ± 0.14	-10.6 ± 1.1
	TAR$^{\Delta U25}$		0.08 ± 0.01	7.13 ± 0.02	-12.3 ± 0.5
	TAR$^{\Delta 23UCU25}$		N.D.		
	TAR$^{G26C/C39G}$		N.D.		
	TAR$^{G28C/C37G}$		N.D.		
	Tat ^{R49A}	TAR^{2GC} WT	0.5 ± 0.2	6.3 ± 0.22	-9.05 ± 0.5
	Tat $^{K50A/K51A}$		0.63 ± 0.14	6.21 ± 0.1	-12.6 ± 0.3
	Tat ^{R52A}		69 ± 9	4.15 ± 0.07	-
	Tat ^{R55F}		0.64 ± 0.22	6.21 ± 0.15	-9.9 ± 0.43
	Tat ^{R55W}		0.95 ± 0.4	6.06 ± 0.23	-9.0 ± 1
	Tat ^{R56A}		0.49 ± 0.3	6.38 ± 0.32	-9.6 ± 2.1
	Tat $^{G48A/Q54A/Q60A}$		0.23 ± 0.01	6.65 ± 0.02	-12.6 ± 1.2
	Tat $^{G48P/Q54P/A58P}$		0.12 ± 0.02	6.91 ± 0.06	-10.7 ± 1.3

Supplementary Table 2. Summary of binding measurements using FP and ITC.
Values are mean ± s.d. of n= 3 biologically independent replicates. N.D.: not determined due to weak binding.

Method	RNA	$[Mg^{2+}]$ (mM)	T_{m1} (ºC)	T_{m2} (ºC)
DSC	TAR^{2GC}	2	78.2	83.0
	TAR^{3G}	2	79.0	-
	TAR^{3GC}	2	80.6	-
	TAR^{GAAA}	2	77.4	83.4
	$TAR^{G16A/A17G}$	2	79.8	-
	$TAR^{G16A/A17G/GAAA/ins59A}$	2	79.8	-
	TAR^{2GC}	0	70.9	78.8
	TAR^{3G}	0	72.4	-
	TAR^{3GC}	0	73.1	-
CD	TAR^{2GC}	0	71.0	-
	TAR^{3G}	0	70.6	-
	TAR^{3GC}	0	74.3	-
	TAR^{2GC}	2	77.9	-
	TAR^{3G}	2	76.5	-
	TAR^{3GC}	2	79.5	-

Supplementary Table 3. Summary of melting parameters by differential scanning calorimetry (DSC) and circular dichroism (CD).

	Full-length HIV-1 TAR-I (TAR^{GAAA})	Full-length HIV-1 TAR-II ($TAR^{G16A/A17G/GAAA/ins59A}$)	Full-length HIV-1 TAR-I + Tat^{44-60}	Full-length HIV-1 TAR-II + Ca^{2+}
Data collection				
Space group	$P2_1$	$P2_12_12$	$P2_1$	$P2_122_1$
Cell dimensions				
a, *b*, *c* (Å)	61.25, 41.98, 68.57	132.54, 32.58, 46.21	68.87, 40.51, 120.41	31.59, 47.26, 132.77
α, β, γ (°)	90, 93.44, 90	90, 90, 90	90, 94.61, 90	90, 90, 90
Resolution (Å) [a]	35.79- 2.35 (2.434 – 2.35)	33.13 – 2.25 (2.331 – 2.25)	40.01 – 2.749 (2.847 – 2.749)	44.53 – 2.761 (2.86 – 2.761)
R_{merge} [a]	0.051 (1.10)	0.135 (1.71)	0.238 (1.70)	0.23.0 (3.51)
$I / \sigma I$ [a]	14.38 (1.63)	7.98 (1.57)	4.89 (1.16)	13.82 (1.62)
$CC_{1/2}$ [a]	0.999 (0.868)	0.991 (0.442)	0.994 (0.711)	0.999 (0.669)
CC* [a]	1 (0.964)	0.998 (0.783)	0.999 (0.912)	1 (0.895)
Completeness (%) [a]	97.46 (97.92)	99.6 (98.69)	97.84 (99.14)	99.17 (95.32)
Redundancy [a]	6.6 (6.3)	7.1 (7.3)	7.4 (7.7)	42.8 (42.1)
Refinement				
Resolution (Å) [a]	35.79- 2.35 (2.434 – 2.35)	33.13 – 2.25 (2.331 – 2.25)	40.01 – 2.749 (2.847 – 2.749)	44.53 – 2.761 (2.86 – 2.761)
No. reflections [b]	97282 (8976)	70998 (7124)	1304418 (13383)	236082 (22373)
R_{work} / R_{free} [a]	0.263/0.282 (0.452/0.505)	0.194/0.222 (0.340/0.376)	0.249/0.288 (0.392/0.436)	0.244/0.294 (0.329/0.405)
No. atoms				
Macromolecule	2320	1188	4762	1174
Water	6	38	9	7
Ligands	66	32	131	1
Mean *B*-factors (Å^2)				
Macromolecule	100.19	54.02	58.14	67.04
Water	88.72	45.18	44.77	52.21
Ligands	99.11	109.16	67.49	62.51
R.m.s. deviations				
Bond lengths (Å)	0.004	0.006	0.002	0.002
Bond angles (°)	1.0	1.39	0.56	0.43
PDB accession code	9DE6	9DE7	9DE5	9DE8

Supplementary Table 4. Summary of crystallographic statistics.

[a] Values in parentheses are for the highest resolution shell.

[b] Values in parentheses are for the cross-validation set.

2AP position	Titrant	Titrant concentration	τ_1 (ns)	Amplitude (A1)	τ_2 (ns)	Amplitude (A2)	τ_3 (ns)	Amplitude (A3)	τ_{avg} (ns)
2AP3	-		0.57	0.55	3.16	0.29	8.96	0.15	2.57
	NC	1 μM	0.54	0.55	3.03	0.29	8.88	0.16	2.59
		2 μM	0.57	0.55	3.16	0.29	9.07	0.15	2.59
		5 μM	0.58	0.55	3.26	0.3	9.14	0.15	2.67
		10 μM	0.59	0.54	3.11	0.3	8.86	0.17	2.76
		20 μM	0.61	0.53	3.19	0.3	8.75	0.17	2.77
		30 μM	0.56	0.57	3.32	0.28	8.84	0.15	2.57
		40 μM	0.37	0.67	2.94	0.21	8.37	0.12	1.87
		50 μM	0.37	0.69	3	0.2	8.35	0.11	1.77
	dsRBMs	1 μM	0.62	0.56	3.06	0.3	8.62	0.15	2.56
		2 μM	0.57	0.58	3.02	0.29	8.75	0.13	2.34
		5 μM	0.54	0.58	2.99	0.29	8.84	0.14	2.41
		10 μM	0.49	0.57	2.86	0.28	8.84	0.15	2.41
		20 μM	0.46	0.57	2.83	0.27	8.94	0.16	2.46
		30 μM	0.52	0.55	3	0.28	9.03	0.17	2.66
		40 μM	0.3	0.74	2.74	0.17	9.03	0.1	1.6
		50 μM	0.22	0.84	2.64	0.1	8.92	0.06	1
	Tat	1 μM	0.54	0.55	3.03	0.29	8.88	0.16	2.60
		2 μM	0.57	0.55	3.16	0.29	9.07	0.15	2.59
		5 μM	0.58	0.55	3.26	0.3	9.14	0.15	2.67
		10 μM	0.59	0.54	3.11	0.3	8.86	0.17	2.76
		20 μM	0.61	0.53	3.19	0.3	8.75	0.17	2.77
		30 μM	0.56	0.57	3.32	0.28	8.84	0.15	2.57
		40 μM	0.37	0.67	2.95	0.21	8.37	0.12	1.87
		50 μM	0.37	0.69	3	0.2	8.35	0.11	1.77
	urea	8 M	0.78	0.45	3.17	0.48	7.65	0.07	2.41
2AP17	-		0.79	0.15	3.66	0.15	9.48	0.7	7.31
	NC	1 μM	0.69	0.17	3.66	0.18	9.25	0.65	6.79
		2 μM	0.71	0.19	3.79	0.2	9.09	0.61	6.44
		5 μM	0.64	0.21	3.42	0.21	8.99	0.57	5.98
		10 μM	0.53	0.27	3.23	0.21	8.79	0.52	5.39
		20 μM	0.65	0.27	3.51	0.22	89	0.5	5.4
		30 μM	0.63	0.27	3.52	0.22	8.72	0.51	5.39
		40 μM	0.63	0.29	3.54	0.23	8.78	0.49	5.3
		50 μM	0.62	0.29	3.66	0.23	8.81	0.48	5.25
	dsRBMs	1 μM	0.81	0.14	3.56	0.17	9.42	0.69	7.22
		2 μM	0.87	0.15	4.39	0.19	9.57	0.66	7.28
		5 μM	0.91	0.14	4	0.2	9.58	0.66	7.25
		10 μM	0.91	0.17	4.3	0.2	9.58	0.66	7.31
		20 μM	0.75	0.17	4.29	0.2	9.6	0.64	7.13
		30 μM	0.82	0.18	4.21	0.19	9.57	0.63	6.98
		40 μM	0.92	0.18	4.23	0.2	9.61	0.62	6.97
		50 μM	0.83	0.17	4.23	0.2	9.56	0.63	7.0
	Tat	1 μM	0.88	0.15	4.3	0.18	9.59	0.67	7.33
		2 μM	0.89	0.15	4.3	0.21	9.6	0.64	7.18
		5 μM	0.65	0.17	3.93	0.21	9.38	0.63	6.84
		10 μM	0.68	0.17	3.84	0.22	9.18	0.61	6.56
		20 μM	0.86	0.19	4.02	0.23	9.12	0.58	6.38
		30 μM	0.7	0.18	3.73	0.24	9.02	0.58	6.25
		40 μM	0.73	0.2	4.03	0.24	9.1	0.55	6.12
		50 μM	0.86	0.21	4.08	0.25	9.06	0.53	6.0
	urea	8 M	0.52	0.45	3.3	0.26	8.44	0.28	3.45
2AP20	-		0.33	0.33	0.7	0.17	6.62	0.13	1.41
	NC	1 μM	0.3	0.72	2.0	0.16	6.9	0.13	1.44

		2 μM	0.36	0.65	2.07	0.2	7.08	0.15	1.71
		5 μM	0.35	0.6	2.05	0.22	7.19	0.18	1.96
		10 μM	0.44	0.56	2.39	0.24	7.51	0.2	2.32
		20 μM	0.44	0.52	2.34	0.24	7.46	0.24	2.58
		30 μM	0.43	0.5	2.34	0.24	7.46	0.26	2.71
		40 μM	0.41	0.47	2.2	0.24	7.26	0.29	2.82
		50 μM	0.46	0.46	2.39	0.24	7.33	0.31	3.06
	dsRBMs	1 μM	0.48	0.65	3.17	0.24	8.83	0.11	2.04
		2 μM	0.47	0.64	3.2	0.25	9	0.11	2.09
		5 μM	0.5	0.68	3.23	0.2	9	0.12	2.06
		10 μM	0.5	0.63	3.23	0.25	9.11	0.12	2.21
		20 μM	0.45	0.64	3.26	0.25	9.37	0.11	2.14
		30 μM	0.52	0.62	3.64	0.27	9.83	0.11	2.39
		40 μM	0.49	0.62	3.63	0.27	10	0.11	2.38
		50 μM	0.5	0.61	3.67	0.28	10.2	0.11	2.45
	Tat	1 μM	0.26	0.74	1.75	0.15	6.57	0.11	1.18
		2 μM	0.28	0.73	1.81	0.15	6.6	0.11	1.2
		5 μM	0.24	0.75	1.75	0.14	6.62	0.11	1.15
		10 μM	0.25	0.74	1.83	0.15	6.67	0.11	1.19
		20 μM	0.16	0.88	1.82	0.07	6.66	0.05	0.6
		30 μM	0.04	0.98	1.52	0.01	6.24	0.01	0.12
		40 μM	0.1	0.94	1.55	0.04	6.09	0.02	0.27
		50 μM	0.06	0.97	1.57	0.02	6.08	0.01	0.15
	urea	8 M	0.54	0.54	2.74	0.22	5.3	0.24	2.17
2AP24	-		0.73	0.34	3.33	0.26	8.27	0.4	4.42
	NC	1 μM	0.69	0.35	3.45	0.26	8.47	0.39	4.44
		2 μM	0.75	0.33	3.43	0.25	8.5	0.42	4.67
		5 μM	0.8	0.26	3.56	0.25	8.75	0.49	5.38
		10 μM	0.73	0.2	3.74	0.26	9.08	0.55	6.11
		20 μM	0.72	0.18	3.39	0.22	8.95	0.6	6.24
		30 μM	0.92	0.2	3.83	0.24	9.05	0.56	6.17
		40 μM	0.8	0.21	3.33	0.24	8.88	0.55	5.85
		50 μM	0.83	0.25	3.55	0.26	8.93	0.49	5.51
	dsRBMs	1 μM	0.8	0.28	3.72	0.27	8.9	0.45	5.23
		2 μM	0.66	0.28	3.52	0.28	9.06	0.45	5.25
		5 μM	0.88	0.25	3.9	0.27	9.31	0.48	5.74
		10 μM	0.68	0.24	3.64	0.26	9.34	0.5	5.9
		20 μM	0.68	0.24	3.8	0.26	9.5	0.5	5.9
		30 μM	0.8	0.21	3.79	0.26	9.45	0.53	6.16
		40 μM	0.78	0.21	3.81	0.27	9.52	0.52	6.14
		50 μM	0.77	0.21	3.81	0.26	9.52	0.52	6.1
	Tat	1 μM	0.76	0.3	3.58	0.26	8.7	0.44	4.99
		2 μM	0.73	0.28	3.5	0.27	8.85	0.45	5.13
		5 μM	0.84	0.22	3.81	0.27	9.3	0.51	5.96
		10 μM	0.74	0.18	3.77	0.27	9.34	0.55	6.29
		20 μM	0.77	0.18	3.92	0.27	9.43	0.55	6.38
		30 μM	0.87	0.17	4.07	0.28	9.5	0.55	6.51
		40 μM	0.75	0.18	3.91	0.28	9.42	0.55	6.41
		50 μM	0.86	0.19	4.14	0.3	9.42	0.51	6.21
	urea	8 M	0.75	0.39	2.8	0.28	4.87	0.32	2.63

Supplementary Table 5. Summary of representative 2-aminopurine (2AP) fluorescence lifetime measurements.

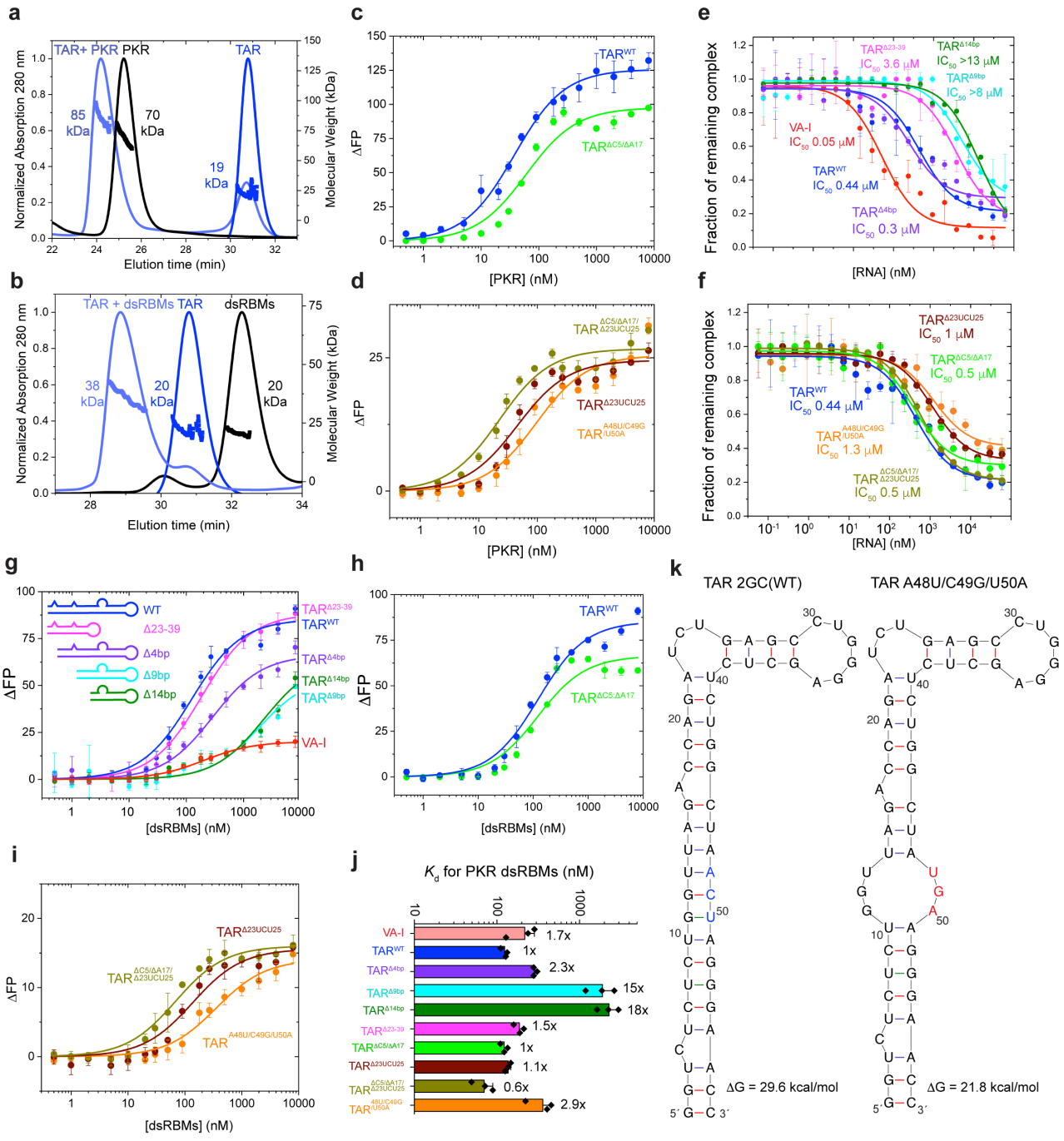
a
TAR+ PKR PKR
TAR
85 kDa
70 kDa
19 kDa
Normalized Absorption 280 nm
Molecular Weight (kDa)
Elution time (min)
b
TAR + dsRBMs TAR
dsRBMs
38 kDa
20 kDa
20 kDa
c
TAR^WT
TAR^ΔC5/ΔA17
ΔFP
[PKR] (nM)
d
TAR^ΔC5/ΔA17/Δ23UCU25
TAR^Δ23UCU25
TAR^A48U/C49G/U50A
e
TAR^Δ23-39 IC50 3.6 μM
TAR^Δ14bp IC50 >13 μM
TAR^Δ9bp IC50 >8 μM
VA-I IC50 0.05 μM
TAR^WT IC50 0.44 μM
TAR^Δ4bp IC50 0.3 μM
Fraction of remaining complex
[RNA] (nM)
f
TAR^Δ23UCU25 IC50 1 μM
TAR^ΔC5/ΔA17 IC50 0.5 μM
TAR^WT IC50 0.44 μM
TAR^A48U/C49G/U50A IC50 1.3 μM
TAR^ΔC5/ΔA17/Δ23UCU25 IC50 0.5 μM
g
WT
Δ23-39
Δ4bp
Δ9bp
Δ14bp
TAR^Δ23-39
TAR^WT
TAR^Δ4bp
TAR^Δ14bp
TAR^Δ9bp
VA-I
[dsRBMs] (nM)
h
TAR^WT
TAR^ΔC5/ΔA17
i
TAR^Δ23UCU25
TAR^ΔC5/ΔA17/Δ23UCU25
TAR^A48U/C49G/U50A
j
K_d for PKR dsRBMs (nM)
VA-I 1.7x
TAR^WT 1x
TAR^Δ4bp 2.3x
TAR^Δ9bp 15x
TAR^Δ14bp 18x
TAR^Δ23-39 1.5x
TAR^ΔC5/ΔA17 1x
TAR^Δ23UCU25 1.1x
TAR^ΔC5/ΔA17/Δ23UCU25 0.6x
TAR^A48U/C49G/U50A 2.9x
k
TAR 2GC(WT)
TAR A48U/C49G/U50A
ΔG = 29.6 kcal/mol
ΔG = 21.8 kcal/mol

Supplementary Fig. 1 | SEC-MALS and FP analyses of TAR interactions with PKR and its dsRBMs.

a Size exclusion chromatography coupled to multi-angle light scattering (SEC-MALS) profiles of full-length PKR (black), HIV-1 TAR (dark blue) and stoichiometric (1:1) mixture of PKR with TAR (light blue). SEC-MALS-derived molecular weights are indicated. **b** SEC-MALS profiles of dsRBMs of PKR (black), TAR (dark blue) and stoichiometric (1:1) mixture of dsRBMs with TAR (light blue). **c, d** Fluorescence polarization (FP) titrations of WT and variant TAR RNAs with full-length PKR. **e, f** Competitive binding experiments where fluorescently labeled WT TAR pre-bound to PKR were challenged by increasing amounts of unlabeled 79-bp dsRNA competitor. Apparent IC_{50}s are indicated. Values are mean ± s.d., n=3 biologically independent samples. **g-i** Fluorescence polarization titrations of VA-I and TAR variants with increasing concentrations of dsRBMs of PKR. **j** Comparisons of dsRBMs-RNA binding affinities obtained from g-i. **k** Mfold[1] analyses of the predicted secondary structures of the WT TAR^{2GC} (left) and A48U/C49G/U50A mutant TAR. The original and new trinucleotides are indicated in blue and red, respectively. Theoretical free energies of RNA folding are also indicated.

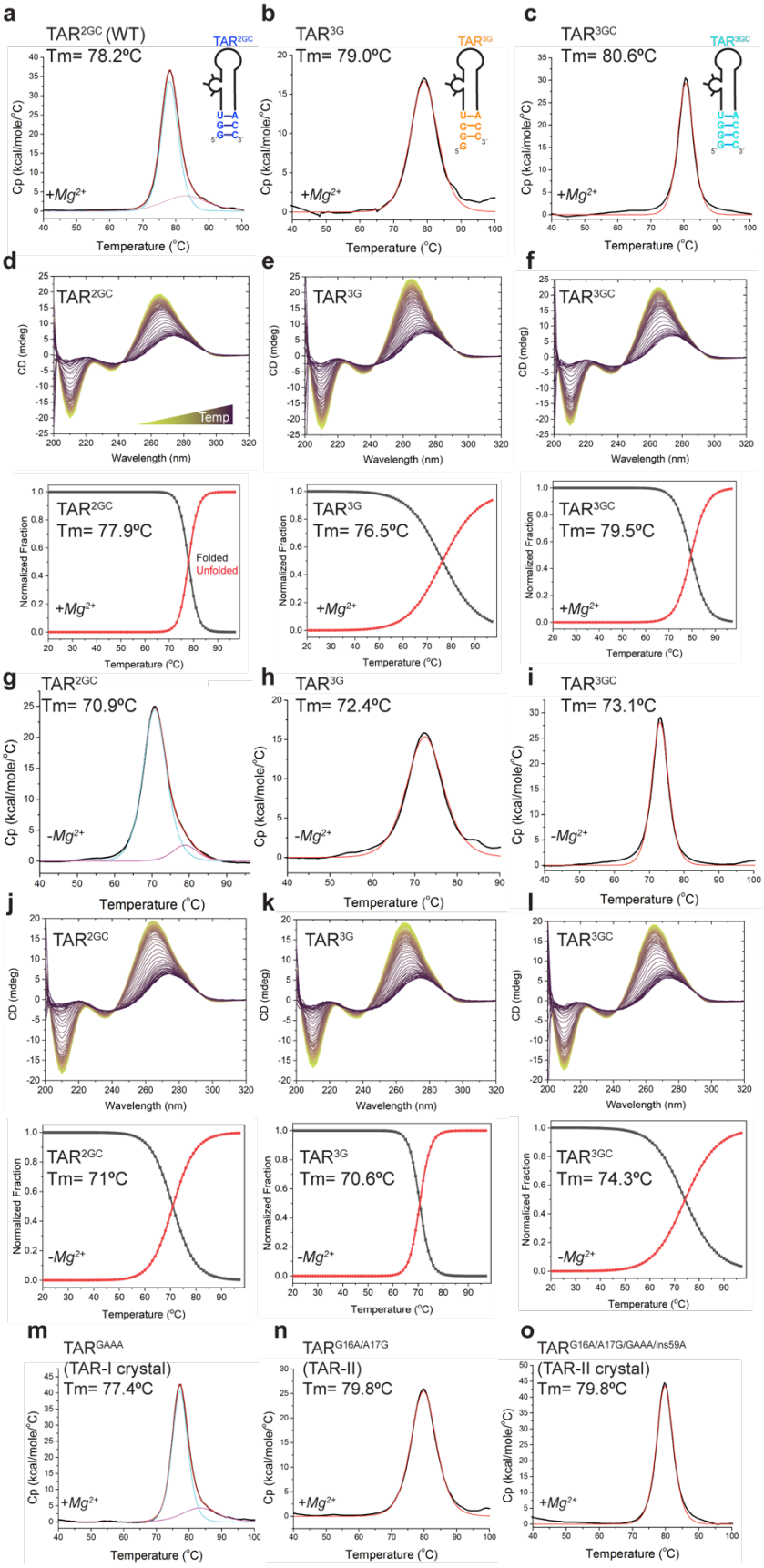
a
TAR2GC (WT)
Tm= 78.2ºC
+Mg2+
Cp (kcal/mole/ºC)
Temperature (ºC)
b
TAR3G
Tm= 79.0ºC
+Mg2+
c
TAR3GC
Tm= 80.6ºC
+Mg2+
d
TAR2GC
Temp
CD (mdeg)
Wavelength (nm)
e
TAR3G
f
TAR3GC
TAR2GC
Tm= 77.9ºC
Folded
Unfolded
+Mg2+
Normalized Fraction
TAR3G
Tm= 76.5ºC
TAR3GC
Tm= 79.5ºC
g
TAR2GC
Tm= 70.9ºC
-Mg2+
h
TAR3G
Tm= 72.4ºC
i
TAR3GC
Tm= 73.1ºC
j
TAR2GC
k
TAR3G
l
TAR3GC
TAR2GC
Tm= 71ºC
TAR3G
Tm= 70.6ºC
TAR3GC
Tm= 74.3ºC
m
TARGAAA
(TAR-I crystal)
Tm= 77.4ºC
n
TARG16A/A17G
(TAR-II)
Tm= 79.8ºC
o
TARG16A/A17G/GAAA/ins59A
(TAR-II crystal)
Tm= 79.8ºC

Supplementary Fig. 2 | DSC and CD analyses of WT and variant TAR thermostabilities. **a-c** DSC profiles of $TAR^{2GC\ (WT)}$ (**a**), TAR^{3G} (**b**) and TAR^{3GC} (**c**) in the presence of 2 mM Mg^{2+}. The measured melting temperatures (T_m) are indicated. **d-f** Upper panels: temperature-scanning CD profiles of TAR^{2GC} (**d**), TAR^{3G} (**e**) and TAR^{3GC} (**f**) collected from 20 to 97°C in 1°C intervals in the presence of 2 mM Mg^{2+}. Lower panels: fractions of folded (black) and unfolded (red) TAR as functions of temperature derived by global fitting of the CD profiles above. **g-i** DSC profiles of TAR^{2GC} (**g**), TAR^{3G} (**h**) and TAR^{3GC} (**i**) in the absence of Mg^{2+}. **j-l** Upper panels: temperature-scanning CD profiles of TAR^{2GC} (**j**), TAR^{3G} (**k**) and TAR^{3GC} (**l**) collected from 20 to 97°C in 1°C intervals in the absence of Mg^{2+}. Lower panels: fractions of folded (black) and unfolded (red) TAR as functions of temperature derived by global fitting of the CD profiles above. **m-o** DSC analyses in the presence of 2 mM Mg^{2+} of TAR^{GAAA} (**m**), $TAR^{G16A/A17G}$ (**n**), and $TAR^{G16A/A17G/GAAA/ins59A}$ (**o**). The measured melting temperatures (T_m) are indicated. Experiments performed once.

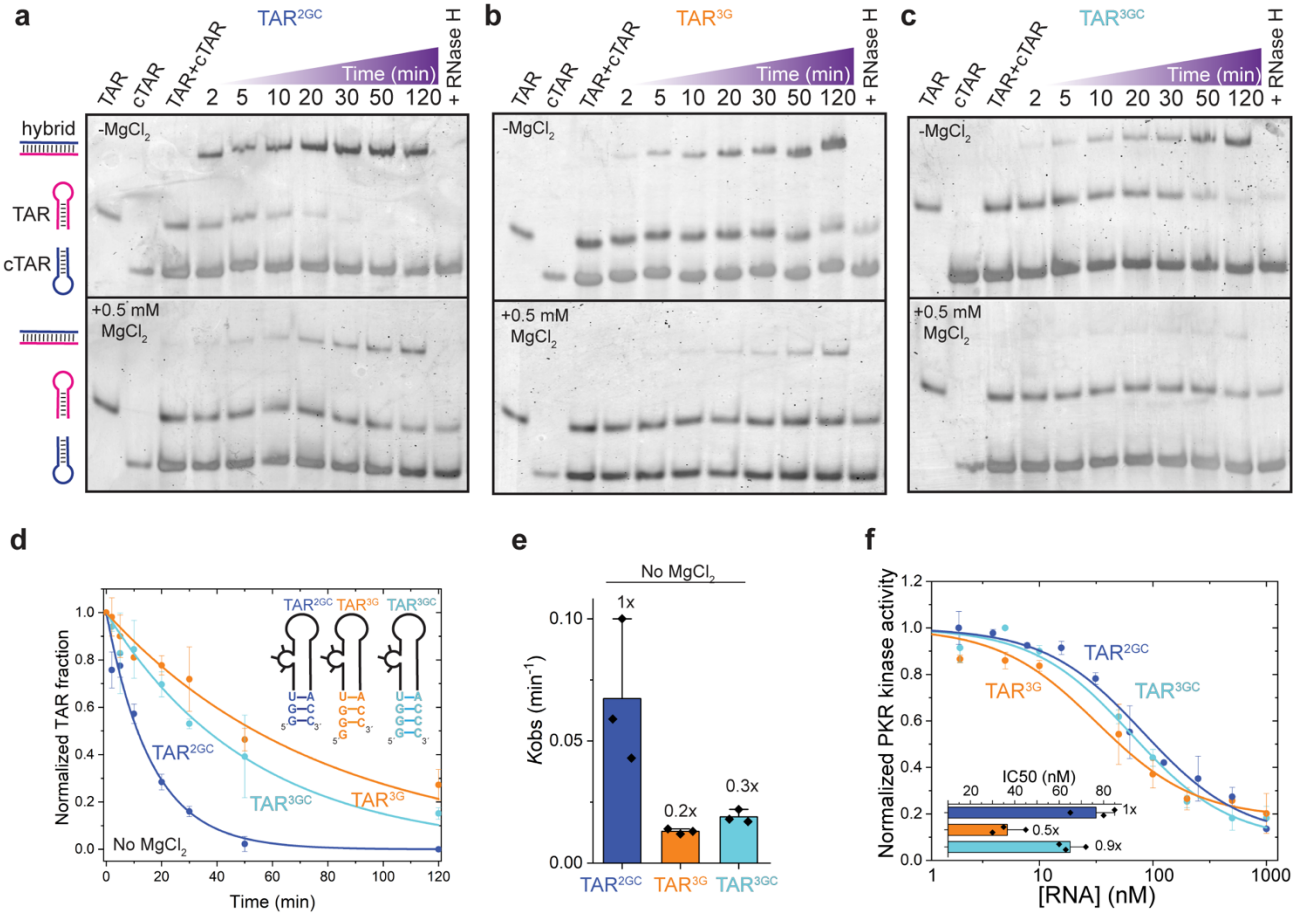

Supplementary Fig. 3 | Effects of TAR 5′ end heterogeneity on TAR-cTAR annealing and PKR inhibition.

a-c Representative non-denaturing PAGE analyses of NC-mediated annealing of cTAR to TAR^{2GC} (**a**), TAR^{3G} (**b**), and TAR^{3GC} (**c**) in the absence (upper panels) or presence (lower panels) of 0.5 mM Mg^{2+}. **d** Plot of the remaining TAR RNA fractions as functions of time in the absence of Mg^{2+} in (a-c). **e** Comparison of the apparent rates of annealing derived from the data in d. **f** PKR-inhibition profiles by TAR^{2GC} (blue), TAR^{3G} (orange) and TAR^{3GC} (cyan). Insert: the derived IC_{50} values. Values are mean ± s.d. of 3 biologically independent replicates.

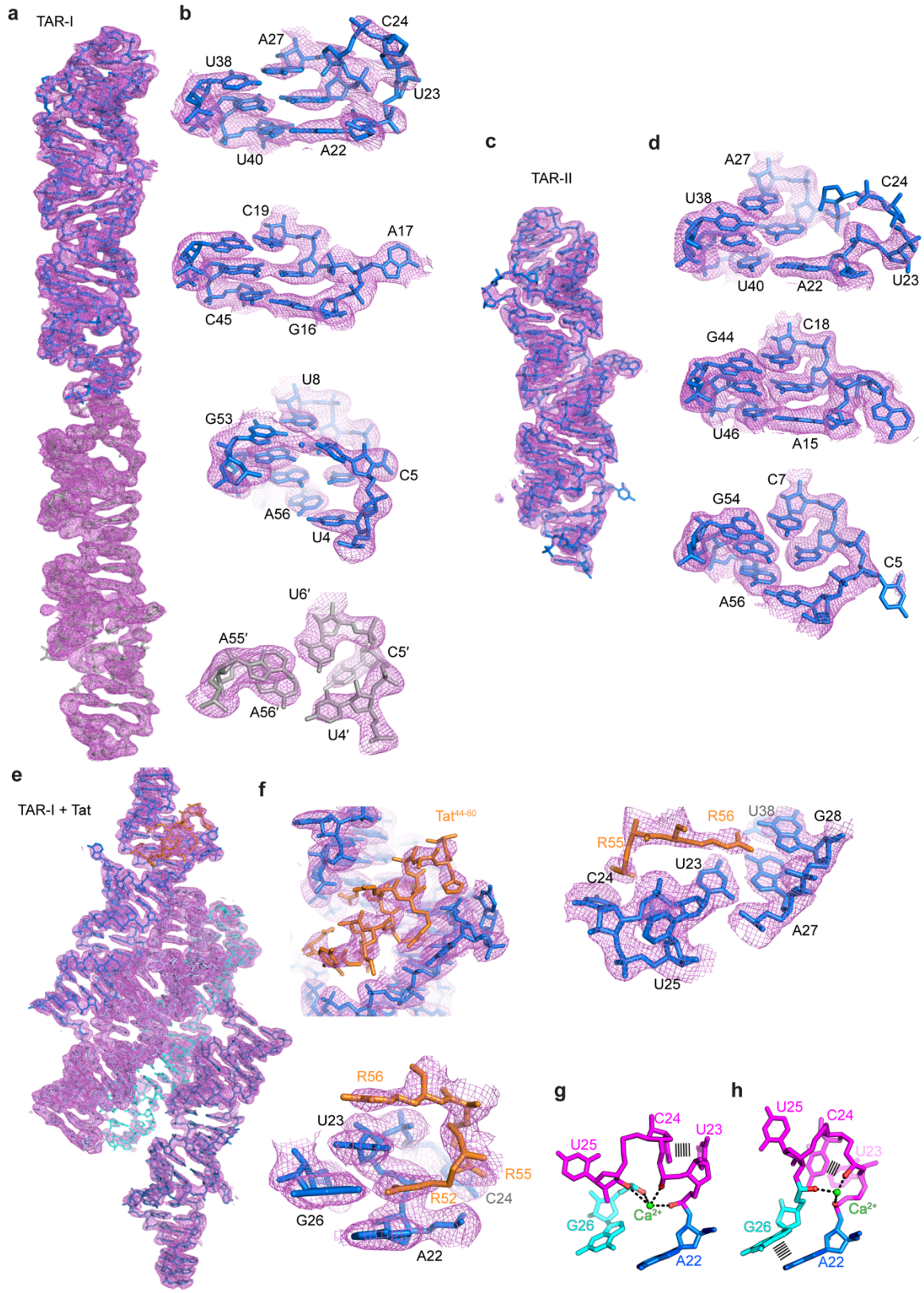
a
TAR-I
b
C24
A27
U38
U23
U40
A22
C19
A17
C45
G16
U8
G53
C5
A56
U4
U6′
A55′
C5′
A56′
U4′
c
TAR-II
d
A27
C24
U38
U40
A22
U23
G44
C18
U46
A15
C7
G54
C5
A56
e
TAR-I + Tat
f
Tat44-60
R56
U38
G28
R55
U23
C24
A27
U25
R56
U23
R55
R52
C24
G26
A22
g
C24
U23
U25
Ca2+
G26
A22
h
U25
C24
U23
Ca2+
G26
A22

Supplementary Fig. 4 | Representative electron densities for TAR-I, TAR-II, and Tat-bound TAR-I crystal structures. a Composite simulated anneal-omit 2Fo-Fc electron densities calculated using the final model and superimposed with the final refined model contoured at 1σ for TAR-I. **b** Four portions of the map in a. Apostrophes denote symmetry-related molecules. **c** Composite simulated anneal-omit 2Fo-Fc electron densities calculated using the final model and superimposed with the final refined model contoured at 1σ for TAR-II. **d** Three portions of the map in c. **e** Composite simulated anneal-omit 2Fo-Fc electron densities calculated using the final model and superimposed with the final refined model contoured at 1σ for TAR-I (blue and cyan) soaked with HIV-1 Tat^{44-60} (orange). **f** Three portions of the map in e**. g** Structure of the UCU bulge in TAR-II soaked with $CaCl_2$. **h** Structure of the UCU bulge in the mini-TAR crystal structure soaked with $CaCl_2$ (PDB:397D)[2].

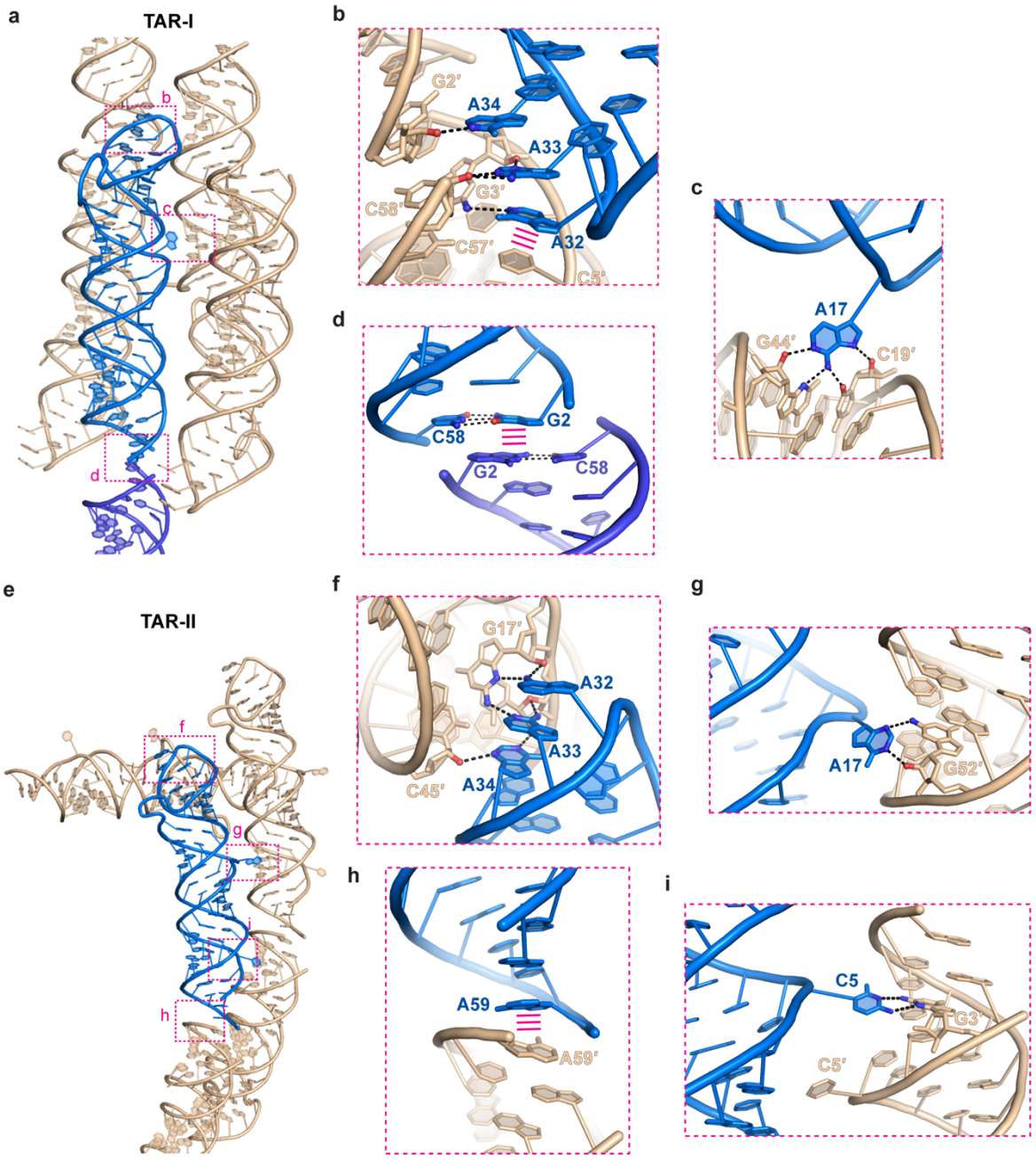

Supplementary Fig. 5 | Crystal-packing arrangements and interfaces in TAR crystals. a Overall crystal-packing arrangements in TAR-I crystals. The reference and symmetry-related molecules are shown in blue and wheat, respectively. **b-d** Detailed crystal-packing interfaces and contacts in the boxes in a. Black dotted lines represent hydrogen bonds and magenta lines indicate stacking interactions. Apostrophes denote symmetry-related molecules. **e** Overall crystal-packing arrangements in TAR-II crystals. **f-i** Detailed crystal-packing interfaces and contacts in the boxes in e. Apostrophes denote symmetry-related molecules.

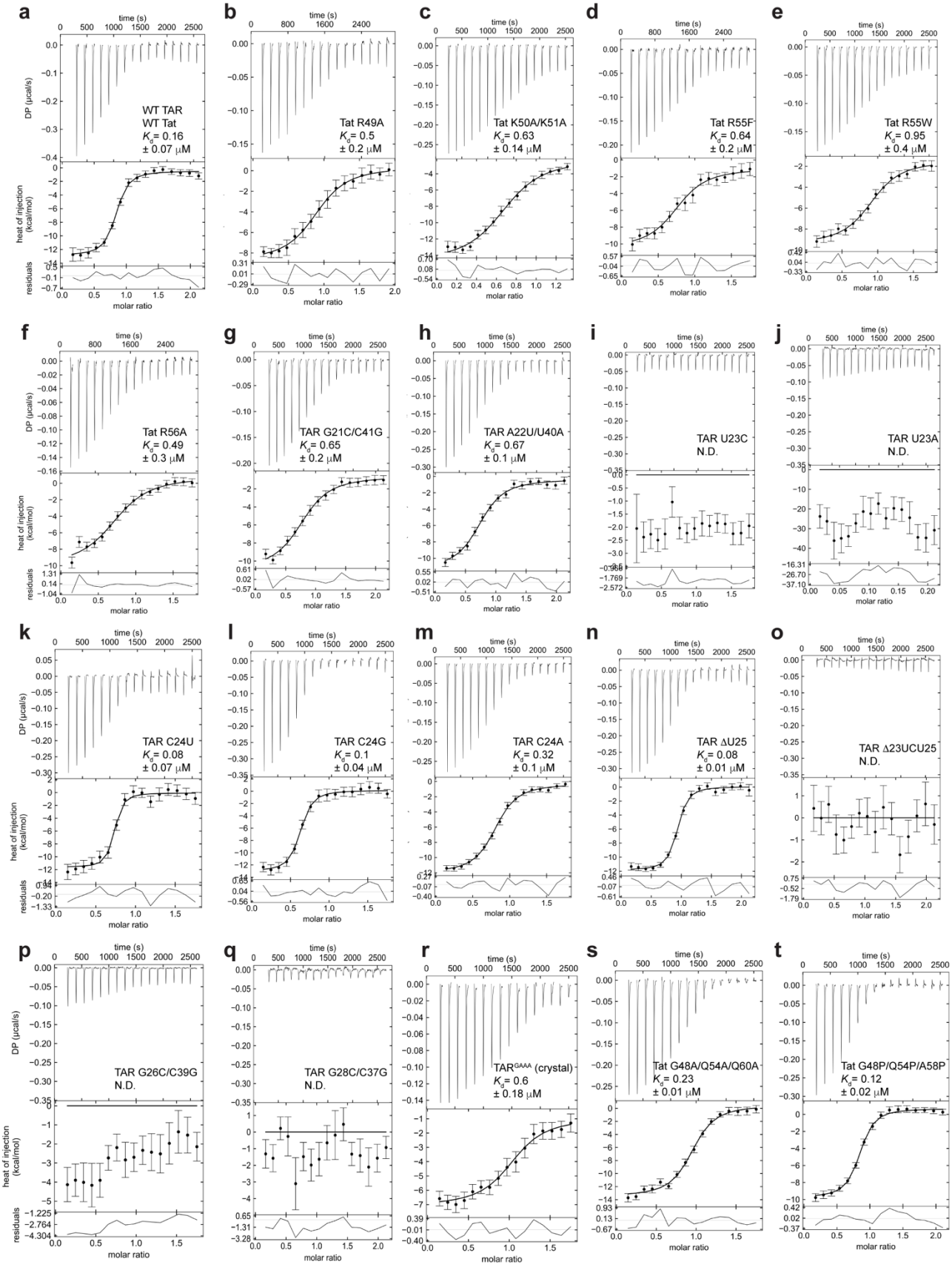
a
WT TAR
WT Tat
K_d= 0.16
± 0.07 μM
b
Tat R49A
K_d= 0.5
± 0.2 μM
c
Tat K50A/K51A
K_d= 0.63
± 0.14 μM
d
Tat R55F
K_d= 0.64
± 0.2 μM
e
Tat R55W
K_d= 0.95
± 0.4 μM
f
Tat R56A
K_d= 0.49
± 0.3 μM
g
TAR G21C/C41G
K_d= 0.65
± 0.2 μM
h
TAR A22U/U40A
K_d= 0.67
± 0.1 μM
i
TAR U23C
N.D.
j
TAR U23A
N.D.
k
TAR C24U
K_d= 0.08
± 0.07 μM
l
TAR C24G
K_d= 0.1
± 0.04 μM
m
TAR C24A
K_d= 0.32
± 0.1 μM
n
TAR ΔU25
K_d= 0.08
± 0.01 μM
o
TAR Δ23UCU25
N.D.
p
TAR G26C/C39G
N.D.
q
TAR G28C/C37G
N.D.
r
TAR^{GAAA} (crystal)
K_d= 0.6
± 0.18 μM
s
Tat G48A/Q54A/Q60A
K_d= 0.23
± 0.01 μM
t
Tat G48P/Q54P/A58P
K_d= 0.12
± 0.02 μM
time (s)
DP (μcal/s)
heat of injection (kcal/mol)
residuals
molar ratio

Supplementary Fig. 6 | Representative ITC isotherms for HIV-1 TAR binding to HIV-1 Tat$^{44-60}$. a-f Representative ITC isotherms for TAR$^{2GC(WT)}$ binding to WT (**a**), R49A (**b**), K50A/K51A (**c**), R55F (**d**), R55W (**e**) and R56A (**f**) Tat$^{44-60}$ variants. **g-r** Representative ITC isotherms for Tat$^{44-60}$ binding to G21C/C41G (**g**), A22U/U40A (**h**), U23C (**i**), U23A (**j**), C24U (**k**), C24G (**l**), C24A (**m**), ΔU25 (**n**), ΔU23UCU25 (**o**), G26C/C39G (**p**), G28C/C37G (**q**) and GAAA (**r**) TAR constructs. **s-t** Representative ITC isotherms for TAR$^{2GC(WT)}$ binding to G48A/Q54A/Q60A (**s**) and G48P/Q54P/A58P (**t**) Tat$^{44-60}$ variants. The constructs names and the K_d values (mean ± s.d., n=3 biologically independent replicates) are indicated in the top panels of the ITC isotherms.

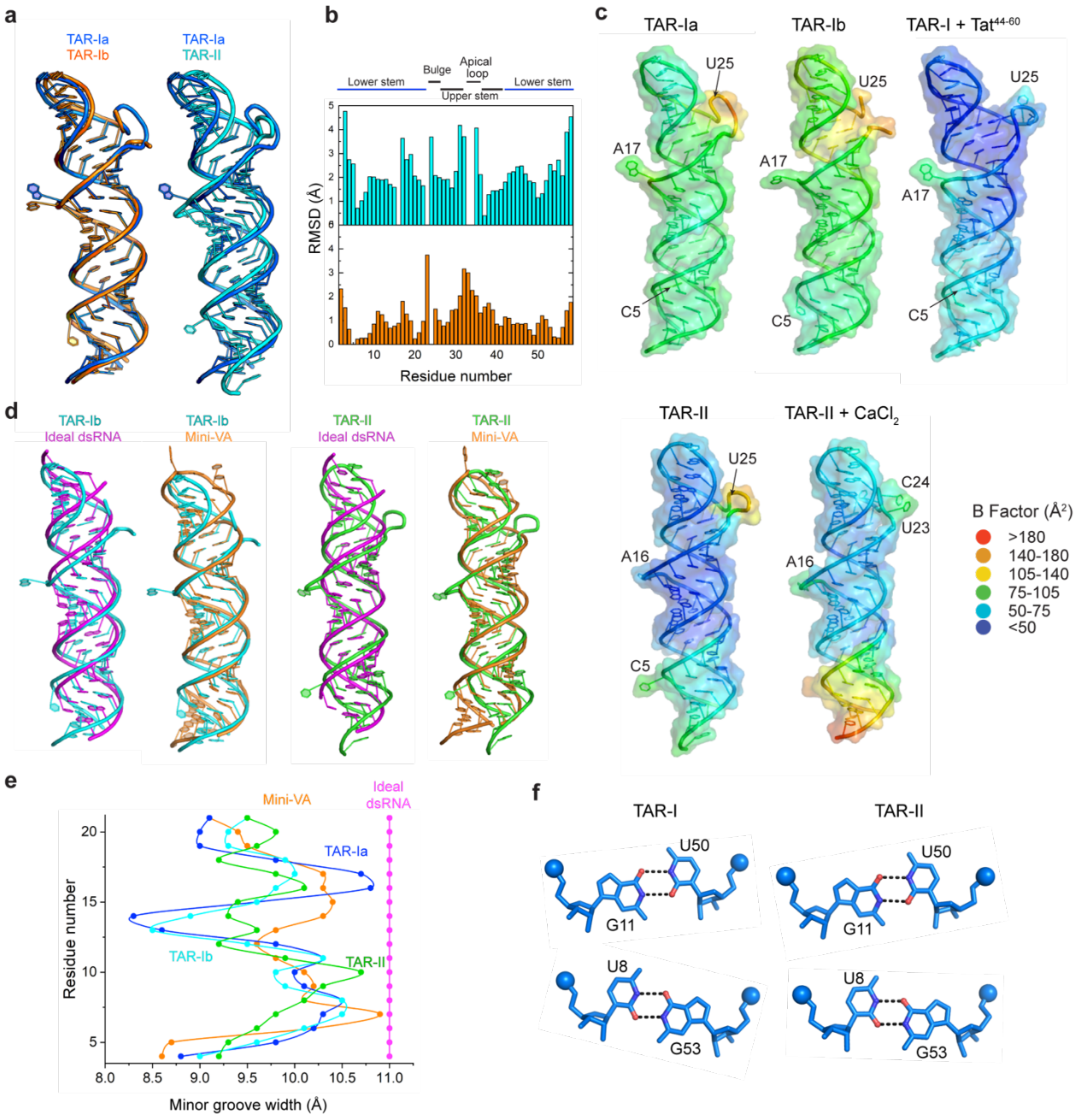

Supplementary Fig. 7 | Comparison of the TAR crystal structures. a Structural overlay of TAR-Ib (orange) and TAR-II (cyan) onto TAR-Ia (blue). **b** Pair-wise root mean square deviations (RMSDs) per residue from a, colored as in a. **c** *B*-factor distributions of TAR structures. **d** Structural overlay of free TAR structures with an ideal A-form dsRNA (magenta) or mini-VA (the fused apical stem-tetrastem of VA-I RNA, orange; PDB: 6OL3[3]). **e** Minor groove widths of RNAs shown in d. **f** G•U wobble base pairs observed in TAR-I (left) and TAR-II (right) crystal structures.

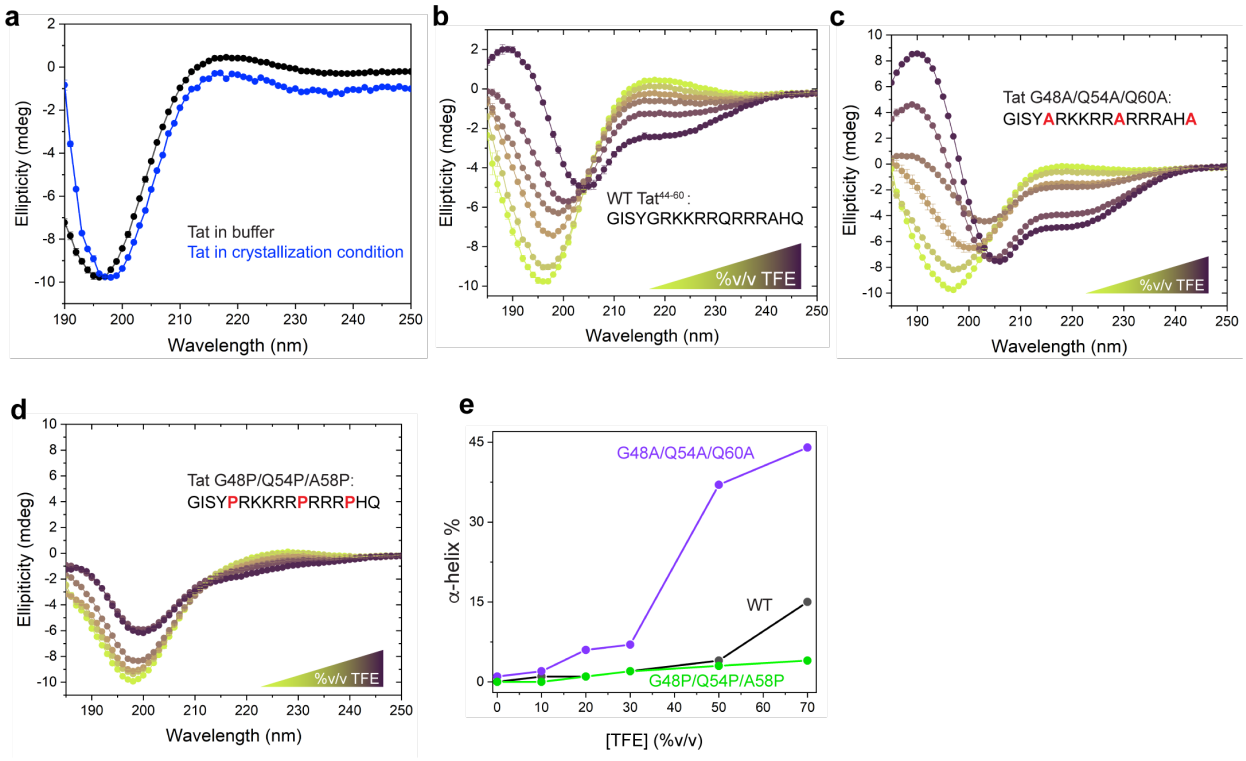

Supplementary Fig. 8 | CD analyses of WT and variant Tat peptides.
a CD spectra of WT Tat$^{44-60}$ in CD buffer (black, 25 mM Tris-HCl pH 7.5 and 25 mM NaCl) or crystallization condition (blue, 25 mM sodium cacodylate pH 6.5, 25 mM NaCl and 50% v/v 2-methyl-2,4-pentanediol). **b-d** CD spectra of WT (**b**), G48A/Q54A/Q60A (**c**), and G48P/Q54P/A58P (**d**) Tat$^{44-60}$ peptides in the presence of increasing concentrations of 2,2,2-Trifluoroethanol (TFE). Peptide sequences are indicated with mutations shown in red. **e** Plot of α-helix percentage in WT and variant Tat$^{44-60}$ in the presence of increasing TFE concentration, derived from CD data in b-d. Experiments performed once.

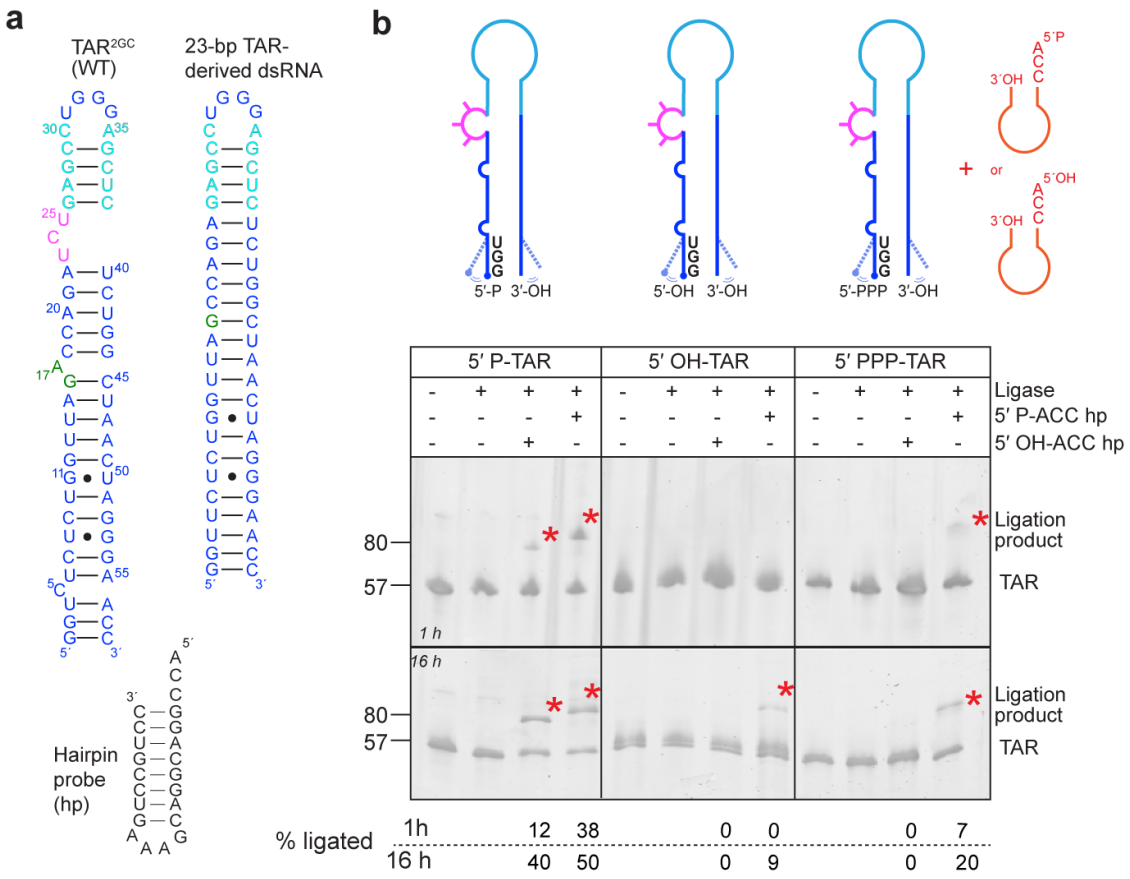

Supplementary Fig. 9 | Additional validation of the RHOALO assay. a Secondary structures of TAR^{2GC} (WT), a TAR-derived 23-bp dsRNA lacking bulged nucleotides, and a hairpin probe used in RHOALO. **b** Cartoon schematics and Urea-PAGE analyses of RHOALO ligation reactions performed using TAR^{2GC} RNAs that harbor 5′ monophosphate, 5′ triphosphate, or 5′ OH groups, and hairpin probes that contain 5′ monophosphate or 5′ OH groups, showing the requirement of 5′-monophosphates for efficient ligation. Red asterisks indicate the ligation products. hp: hairpin. The RNA lengths are indicated in nucleotides. Ligation efficiency is indicated below the gels. Experiments performed once.

.

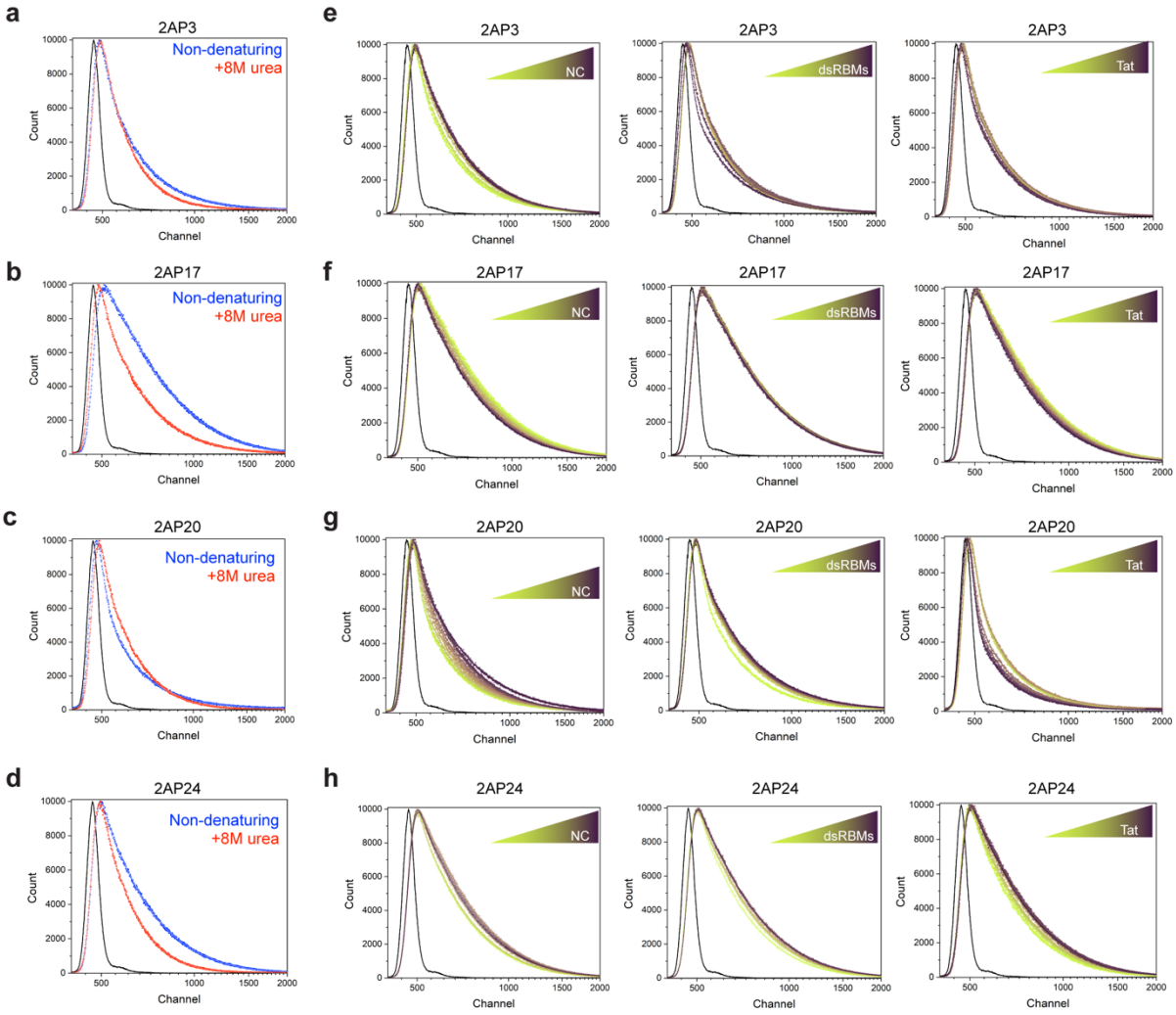

Supplementary Fig. 10 | 2AP TCSPC (Time Correlated Single Photon Counting) time traces. **a-d** Representative time-resolved fluorescence intensity decay profiles of 2AP at position 3 (**a**), position 17 (**b**), position 20 (**c**) and position 24 (**d**) in free TAR^{2GC}, under non-denaturing conditions (blue) or in 8M urea (red). **e-h** Representative time-resolved fluorescence intensity decay profiles of 2AP at position 3 (**e**), position 17 (**f**), position 20 (**g**) and position 24 (**h**) of TAR^{2GC} in the presence of increasing concentrations (from green to brown) of NC (left), dsRBMs of PKR (middle) or Tat (right). n=3 biologically independent replicates.

Supplementary References:

1. Zuker, M. Mfold web server for nucleic acid folding and hybridization prediction. *Nucleic Acids Res* **31**, 3406-15 (2003).
2. Ippolito, J.A. & Steitz, T.A. A 1.3-A resolution crystal structure of the HIV-1 trans-activation response region RNA stem reveals a metal ion-dependent bulge conformation. *Proc Natl Acad Sci U S A* **95**, 9819-24 (1998).
3. Hood, I.V. et al. Crystal structure of an adenovirus virus-associated RNA. *Nat Commun* **10**, 2871 (2019).